ENHANCED-RESOLUTION SMAP SOIL MOISTURE USING IMAGE RECONSTRUCTION

David G. Long

Brigham Young University
Electrical and Computer Engineering Dept.
458 CB, Provo, UT 84604 long@ee.byu.edu

Mary J. Brodzik, Molly Hardman

CIRES/University of Colorado, Boulder
National Snow and Ice Data Center
Boulder, CO 80309 brodzik@nsidc.org

ABSTRACT

The loss of the active sensor channels limits the spatial resolution capability of the Soil Moisture Active Passive (SMAP) mission in measuring soil moisture. Image reconstruction techniques can provide an enhanced resolution product. Using such processing techniques and code developed for the NASA MEaSUREs Calibrated Passive Microwave Daily Equal-Area Scalable Earth (EASE) Grid 2.0 Brightness Temperature (CETB) Earth System Data Record (ESDR) project, we are generating enhanced-resolution SMAP TB products on both 3 km SMAP project grids and 3.125 km CETB-compatible grids. The intrinsic tradeoff between resolution and noise is explored using multiple resolution enhancement algorithms, and the spatial response functions for each are presented.

Index Terms— SMAP, radiometer, reconstruction, resolution enhancement, Backus-Gilbert, passive microwave remote sensing

1. INTRODUCTION

The L-band SMAP radiometer retrieves brightness temperature (T_B) measurements of the Earth's surface [5]. For each of the four Stokes polarizations measured (vertical [V], horizontal [H], and the cross-polarizations 3 and 4), multiple T_B measurements of each point in the 900 km wide swath are collected from several different azimuth angles from which T_B images can be generated. From these, the surface soil moisture is estimated. The 47 km by 36 km footprint limits the effective spatial resolution in conventional processing. However, a number of resolution enhancement techniques have been developed that can improve the effective resolution of the T_B images [6]. Soil moisture is then estimated at finer resolution from the T_B images.

This paper focuses on the generation of enhanced-resolution T_B images. Several resolution enhancement algorithms are compared, and the tradeoffs between spatial resolution and noise are considered with the aid of simulation. Finally, the spatial response function (SRF) for each technique is presented.

2. RESOLUTION ENHANCEMENT THEORY

For all the algorithms considered, the effective spatial measurement response function (MRF) for each measurement is used to estimate the surface T_B on a fine-scale grid. The MRF is determined by the antenna gain pattern, the scan geometry (notably the antenna scan angle), and the integration period that 'smears' the antenna gain pattern due to antenna rotation over the measurement integration period [6]. The MRF for a particular polarization is denoted by $R(\phi, \theta; \phi_i)$, where ϕ and θ are particular azimuth and elevation angles relative to the antenna boresite at azimuth scan angle ϕ_i. Then, assuming the surface emission and atmospheric contributions are azimuthally isotropic, the atmospheric-corrected measurement T_i is the weighted average of the surface T_B where the weighting function is the MRF

$$T_i = \iint R(x, y; \phi_i) T_B(x, y) dx dy + noise, \qquad (1)$$

where $T_B(x, y)$ is the nominal T_B in the direction of point x, y on the surface as observed from the scan angle ϕ_i. The goal in resolution enhancement is to estimate $T_B(x, y)$ on a fine grid from the measurements T_i.

In this paper, two resolution enhancement algorithms are considered: Backus-Gilbert interpolation (BGI) [1] and the radiometer form of the scatterometer image reconstruction algorithm (rSIR) [6, 7]. The latter is a particular example of a signal reconstruction algorithm (SRA). While in practice the results are broadly similar, BGI and SRAs are based on fundamentally different approaches and assumptions about the signals (the surface T_B and its measurements) involved.

BGI is a least-squares approach that explicitly trades noise and solution smoothness using a subjectively selected parameter [1]. Making no assumptions about the signal or the sampling, BGI attempts to minimize the squared difference between the measurements and the forward projection of the signal. An SRA such as rSIR is based on signal processing. SRAs exploit oversampling of the surface to reconstruct images at fine spatial resolution, and hence they can be considered resolution enhancement algorithms, though technically they just recover existing information. SRAs assume that the signal to be reconstructed is bandlimited and the sampling

(measurement locations) meets generalized Nyquist requirements for the signal bandwidth. An additional requirement is that the frequency response of the MRF is non-zero over the signal bandwidth [4]. This reconstructs the original signal from the samples (measurements), and can exactly estimate the original bandlimited signal in the noise-free case. In contrast, BGI cannot guarantee an exact estimate even in the noise-free case unless the sampling and MRF also meet the SRA requirements.

Since the T_B measurements are quite noisy, a full reconstruction can produce excessively noisy estimates of the surface T_B [6]. To reduce noise enhancement and resulting artifacts, regularization is employed. Regularization is a smoothing constraint introduced to an inverse problem to prevent extreme values or overfitting, but it has the side effect of reducing resolution because the image estimate is only a partial reconstruction. The regularization in rSIR enables a tradeoff between signal reconstruction accuracy and noise enhancement and is imposed by limiting the number of iterations of the algorithm.

Our interest in this paper is with an Earth-based grid (map) rather than swath coordinates. In some cases (notably in the polar regions), multiple passes over the same area at the same local time of day can be averaged together. This improves the sampling density, and hence the reconstruction capability. The measurement locations are not aligned with the grid and the measurements form an irregular sampling pattern for T_B. To address this, the well-defined theory of signal reconstruction based on irregular sampling [2, 3] is employed to understand the recoverable signal given the sampling density [6].

To briefly describe the reconstruction theory, the two-dimensional T_B over an $N_x \times N_y$ pixel grid is written as a single dimensional variable $a_j = T_B(x_j, y_j)$, where $j = l + N_x k$. The measurement equation, Eq. 1, becomes

$$T_i = \sum_{j \in \text{image}} h_{ij} a_j \tag{2}$$

where $h_{ij} = R(x_l, y_k; \phi_i)$ is the discretely sampled MRF for the i-th measurement evaluated at the j-th pixel center, and the summation is over the image with $\sum_j h_{ij} = 1$. Written as a matrix equation for the collection of measurements, this is

$$\vec{T} = \mathbf{H}\vec{a} \tag{3}$$

where $\mathbf{H}$ contains the sampled MRF for each measurement and $\vec{T}$ and $\vec{a}$ are vectors composed of the measurements T_i and the sampled surface T_B a_j, respectively. The matrix $\mathbf{H}$ is very large, sparse, and may be overdetermined or underdetermined depending on the sampling density. Estimating the brightness temperature at high resolution is equivalent to inverting Eq. 3 (with bandlimit constraints in the SRA case).

rSIR is a particular implementation of an iterative solution to Eq. 3 that has proven effective in generating high-resolution brightness temperature images [6, 7]. It can handle single or multiple pass cases. The rSIR estimate approximates a maximum-entropy solution to an underdetermined equation and a least-squares solution to an overdetermined system. The first iteration of rSIR is termed 'AVE' (for weighted AVErage). The AVE estimate of the j-th pixel is given by

$$a_j = \frac{\sum_i h_{ij} T_i}{\sum_i h_{ij}} \tag{4}$$

where the sums are over all measurements that have non-negligible MRF at the pixel. Later iterations update the image using the ratio of the forward projections and the measurements [6].

The Backus and Gilbert approach to inverting Eq. 3 is based on writing the estimated T_B value at the j-th pixel as the weighted linear sum of nearby T_B measurements,

$$\widehat{a_j} = \sum_{i \in \text{nearby}} w_{ij} T_i \tag{5}$$

where the weights w_{ij} are selected so that $\sum_i w_{ij} = 1$. With no unique solution for the weights, regularization enables a subjective tradeoff between noise level and resolution [7]. For a particular pixel j the total squared signal reconstruction error term Q_R is

$$Q_R = \left(\sum_{j \in nearby} w_{ij} h_{ij} - 1 \right)^2 \tag{6}$$

with the error due to noise Q_N given by

$$Q_N = \vec{w}^T \mathbf{E} \vec{w} \tag{7}$$

where $\mathbf{E}$ is the noise covariance matrix. A parameter γ weights the reconstruction error and the noise error in the total error Q:

$$Q = Q_R \cos\gamma + \omega Q_N \sin\gamma \tag{8}$$

where ω is an arbitrary dimensional tuning parameter. When the noise realization is independent from measurement to measurement, $\mathbf{E}$ is a diagonal matrix with diagonal entries $\Delta T/2$ where ΔT is the radiometer channel noise standard deviation. Minimizing the total error Q, the weight vector is

$$\vec{w} = \mathbf{Z}^{-1} \left(\vec{v} \cos\gamma + \frac{1 - \vec{u}^T \mathbf{Z}^{-1} \vec{v} \cos\gamma}{\vec{u}^T \mathbf{Z}^{-1} \vec{u}} \vec{u} \right) \tag{9}$$

where

$$\begin{aligned} \vec{u}_i &= \sum_j h_{ij} = \vec{v}_i \\ \mathbf{Z} &= \mathbf{G}_j \cos\gamma + \omega \mathbf{E} \sin\gamma \\ (\mathbf{G}_j)_{i,k} &= h_{ij} h_{kj}. \end{aligned}$$

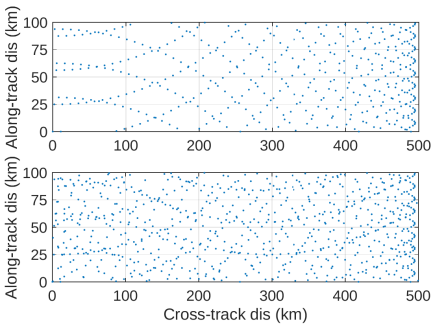

Fig. 1. Simulated SMAP T_B measurement locations on swath grid. (top) Single pass. (bottom) Two passes.

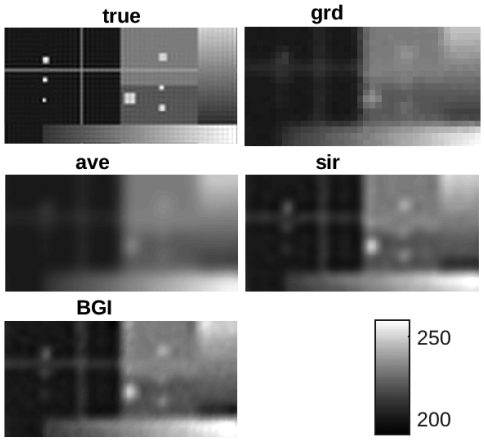

Fig. 2. Comparison of different reconstructions.

3. ALGORITHM COMPARISON

To evaluate and compare the performance of BGI and rSIR, simulation is employed. A 5 km bandlimited synthetic "truth" image is defined and simulated noisy T_B measurements computed using the SMAP MRF and sampling geometry. The noise standard deviation is set to $\Delta T = 1$ K. The SMAP measurement locations for the 250 km $\times$ 500 km study area are shown in Fig. 1. An example of the simulation results are shown in Fig. 2, which compares the truth image, drop-in-the-bucket (DIB) gridding on a 25 km grid (grd), AVE, rSIR, and BGI using a fine pixel resolution of 3.125 km. Note the finer details evident in the rSIR and BGI images compared to AVE and grd. Also note the higher noise level in the BGI image and the coarse resolution of the grd image.

To determine the "optimum" γ value, images for various γ values are computed. The total error versus γ is shown in Fig. 3. There is a particular value of γ that minimizes the total RMS error. This value is used in Fig. 2. For rSIR, the error is computed for each iteration and plotted in Fig. 4. The RMS signal reconstruction error reduces with iteration, while the noise error increases, see Fig. 5. The minimum total error occurs at rSIR iteration 85 (which is off the plot). Since rSIR has smaller error than the optimum BGI when more than 18 iterations are used, any value larger than 18 can be used.

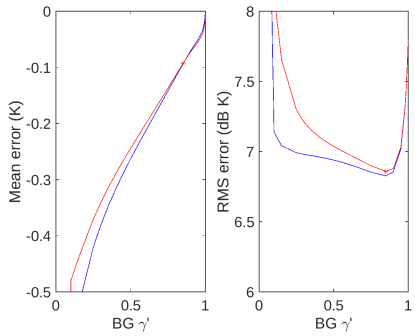

Fig. 3. BGI error versus $\gamma' = 2\gamma/\pi$. The red (upper) curves are for noisy measurements while the blue (lower) curves are for noise-free measurements. ($\mathbf{E}$ is the same in both cases.)

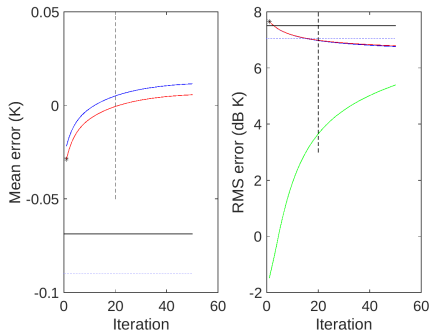

Fig. 4. rSIR error versus iteration. Red is signal+noise case, blue is signal-only. (left) Mean T_B . (Right) RMS T_B . Green is noise-only. The horizontal black line shows the grd error for comparison, while the dotted horizontal line shows the BGI error. The vertical dashed line is at 20 iterations.

However, if rSIR is iterated too long, beyond $\sim$150, the noise error begins to dominate the signal error.

Of critical importance in comparing the algorithms is the spatial response function (SRF), effectively the impulse response. The more "delta" function-like the SRF, the finer the effective resolution. The estimated SRFs for each case in Fig. 2 are shown in Fig. 6 for the 25 km gridded GRD product, AVE, BGI, and rSIR SRF estimates. These have been normalized to a peak of one for comparison. The effective 3 dB resolution of the non-enhanced, and AVE SRFs are similar, though the roll-off of AVE is faster. rSIR has a somewhat finer 3 dB resolution but significantly faster roll-off than AVE or the GRD SRFs. Both BGI and rSIR include negative-valued rings around the center peak. This is not surprising since the sampling limits the bandwidth of the SRF. While the BGI SRF is more localized than grd or AVE, the BGI 3 dB contour is larger than rSIR, implying that rSIR provides somewhat finer resolution than rSIR. The finer resolution is confirmed by examining the spectra of the SRFs (not shown) for which rSIR has the largest region of support in the spatial frequency domain.

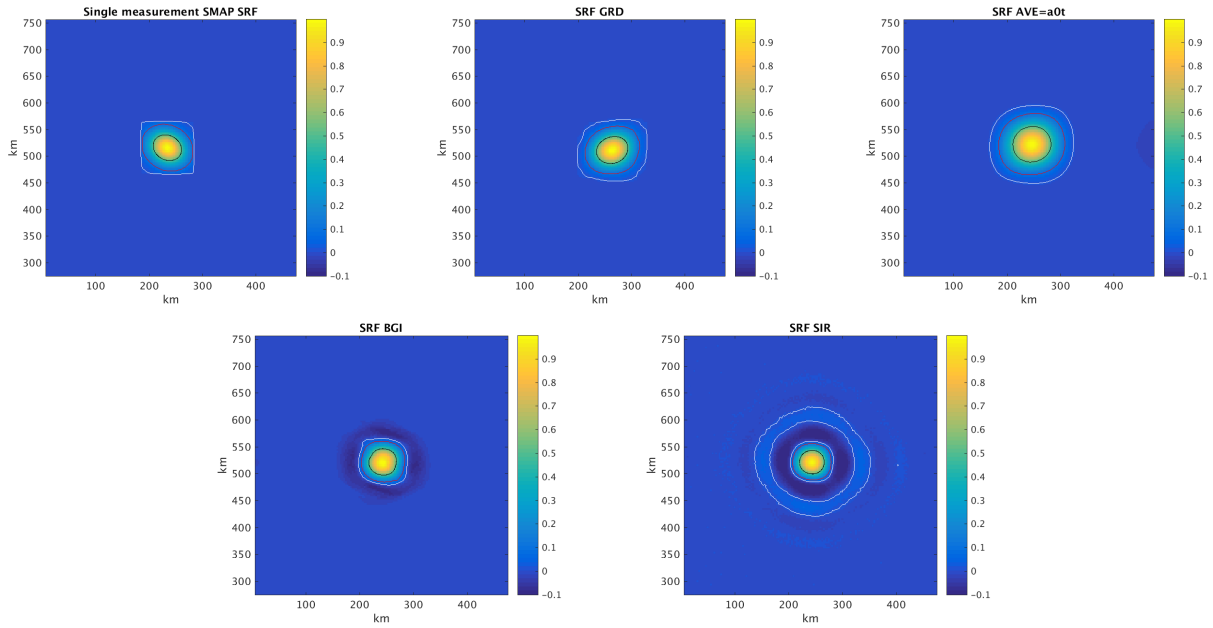

Fig. 6. Images of SRF estimates compared to a single measurement response function. The GRD and AVE SRFs are computed as weighted sums of the measurement response functions, while the BGI and rSIR SRFs are numerically determined by simulating measurements of a bandlimited delta function image. Contours are at (black) -3 dB, (red) -10 dB, and (white) -20 dB.

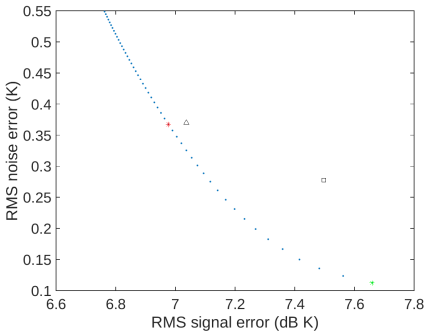

Fig. 5. RMS signal versus noise as a function of rSIR iteration number. Iterations increase from right to left. 25 km DIB is the box at the right, while BGI is the triangle. The red star on the curve is rSIR at 20 iterations, the value used in Fig. 2.

4. SUMMARY

Both BGI and rSIR are effective at improving the resolution of SMAP T_B images, though rSIR requires significantly less computation [6] and, based on simulations, provides slightly better performance. To support the SMAP project, EASE-Grid 2.0 T_B images will be produced at 3 km, nested in the 36 km SMAP grids. SMAP T_B images will also be produced at 25 km and 3.125 km resolution on CETB grids.

5. REFERENCES

[1] G.E. Backus and J.F. Gilbert, Numerical applications of a formalism for geophysical inverse problems, *Geophys. J. R. Astron. Soc.*, vol. 13, pp. 247–276, 1967.

[2] H. Feichtinger and K. Gröchenig, Iterative reconstruction of multivariate band-limited function from irregular sampling values, *SIAM J. Math. Analysis*, vol. 23, no. 1, pp. 244–261, 1992.

[3] K. Gröchenig, Reconstruction algorithms in irregular sampling, *Math. Comp.*, vol. 59, no. 199, pp. 181–194, 1992.

[4] D.S. Early and D.G. Long, Image reconstruction and enhanced resolution imaging from irregular samples, *IEEE Trans. Geosci. Remote Sensing*, vol. 39, no. 2, pp. 291–302, 2001.

[5] J. Piepmeier, P. Mohammed, G. De Amici, E. Kim, J. Pen and C. Ruff, Algorithm theoretical basis document: SMAP calibrated, time-ordered brightness temperatures L1B_TB data product, SMAP Project, Rev. A, 10 Dec 2014.

[6] D.G. Long and M.J. Brodzik, Optimum image formation for spaceborne microwave radiometer products, *IEEE Trans. Geosci. Rem. Sensing*, vol. 54, no. 5, pp. 2763-2779, 2016.

[7] D.G. Long and D.L. Daum, Spatial resolution enhancement of SSM/I data, *IEEE Trans. Geosci. Rem. Sensing*, vol. 36, no. 2, pp. 407-417, 1998.